Submitted to ADVANCED MATERIALS

Supplemental Materials and Methods

Programmable Microfluidic Synthesis of Over One Thousand Uniquely Identifiable Spectral Codes

H.Q. Nguyen[a,+], B.C. Baxter[a,+], K. Brower[b], C.A. Diaz-Botia[a], J.L. DeRisi[a,c], P.M. Fordyce[b,d,e*], and K.S. Thorn[a*]

[a]Department of Biochemistry and Biophysics, University of San Francisco, San Francisco, CA, 94158-2517, USA.
[b]Department of Bioengineering, Stanford University, Stanford, CA, 94305, USA.
[c]Howard Hughes Medical Institute, Chevy Chase, MD, 20815, USA.
[d]Department of Genetics, Stanford University, Stanford, CA, 94305, USA.
[e]ChEM-H, Stanford University, Stanford, CA, 94305, USA.
[+]These authors contributed equally to this work.
[*]Corresponding authors: kthorn@ucsf.edu, pfordyce@stanford.edu

Table of Contents

Additional Information
1. Supplemental Methods (pp. 1 – 3)

Tables
1. Table S1: Lanthanide standard deviation versus mean.
2. Table S2: Summary of MRBLE code sets in this work.

Figures
1. Figure S1: Lanthanide spectrum pre- and post-normalization and nanophosphor size information.
2. Figure S2: Microfluidic MRBLE production schematic.
3. Figure S3: Scatter plot of the 106 MRBLE code set.
4. Figure S4: SD vs lanthanide mean plots.
5. Figure S5: Scatter plot of the 285 MRBLE code set.
6. Figure S6: Scatter plot of the 341 MRBLE code set.
7. Figure S7: Histogram of measured lanthanide ratios for 550 MRBLE code set.
8. Figure S8A: Histogram for reference Eu levels in the 1023 MRBLE code set.
9. Figure S8B: Varied reference Eu levels in the 1101 MRBLE code set.
10. Figure S9: Scatter plot of the 551 codes comprising the low Eu level of the 1101MRBLE set.
11. Figure S10: Scatter plot of 341 Code set from 25% Eu level from 1023-code MRBLE.
12. Figure S11: Scatter plot of 341 Code set from 50% Eu level from 1023-code MRBLE.
13. Figure S12: Scatter plot of 341 Code set from 100% Eu level from 1023-code MRBLE.
14. Figure S13: Microfluidic wafer fabrication schematic and protocols.

Additional Data and Resources
AutoCad files are available upon request from the authors.

Supplementary References
A list of supplemental references accompanying methods and figures.

Section 1: Supplemental Methods

Reagents

Chemical reagents were purchased from Sigma-Aldrich (St. Louis, MO) and were used without further purification. Lanthanide nanophosphor (LN) excitation and emission spectra were measured with a FluoroMax-3 (Horiba Scientific, Kyoto, Japan) spectrofluorometer and the LN particle size distributions were measured with a Zetasizer Nano (Malvern Instruments, Malvern, UK). Lithium phenyl-2,4,6-trimethyl-benzoyl-phosphinate (LAP) was synthesized according to a published protocol[1].

Lanthanide synthesis

Preparation of YVO_4: RE Nanophosphors[2,3]: Solutions (0.1 M) of the rare-earth (RE) dopants [$Sm(NO_3)_3$, $Dy(NO_3)_3$, $Eu(NO_3)_3$, $Tm(NO_3)_3$,], $Y(NO_3)_3$, and Na_3VO_4 were prepared beforehand. A solution of $Y(NO_3)_3$ (2850 µL) and the RE solution (e.g., $Eu(NO_3)_3$) (150 µL) was mixed and then added to a microwave vessel containing 3 mL of H_2O at room temperature. This solution was stirred for 5 minutes, followed by the rapid addition of the Na_3VO_4 solution (2850 µL), when a white precipitate develops. The suspension was transferred into a glass vial suitable for microwave synthesis and was heated to 180 °C at 15 bar for 90 min. The material was pelleted in a 15 mL disposable centrifuge tube and the supernatant was removed. The pellet was then re-suspended in 3 mL of deionized H_2O, to which was added 5 mL of a 10 w/w% PAA solution (Mn ~ 1,400). This mixture was heated to 70 °C and stirred for 10 min. The solution was pH adjusted to 8.5 using 6 N NaOH and stirred for an additional 20 min. The suspension was then diluted 1:10 with deionized H_2O and sonicated for 2 hours. After sonication, the solution was filtered through a 0.45 µm PVDF filter before being added to an ultracentrifugation filter unit (Amicon, 30,000 MWCO) for concentration and the removal of excess salts and polymers. After the entire reaction volume (~100 mL) had been passed through the membrane, the retained nanophosphors were washed 4 times with 15 mL of deionized water to exchange out the remaining solution. The final NP suspensions were milky white in appearance and had a nanophosphor concentration of about 50 mg/mL. Sm-, Dy-, and Eu-doped YVO_4 nanoparticles are all doped at 5% RE substitution for yttrium. YVO_4:Tm is doped at 1%.

Preparation of $La_{0.40}Ce_{0.45}Tb_{0.15}PO_4$ Nanophosphors[4]*:* Solutions (0.1 M) of $LaCl_3$, $CeCl_3$, $TbCl_3$, and $Na_5P_3O_{10}$ were prepared beforehand. First, 1200 µL $LaCl_3$, 1350 µL $CeCl_3$, and 450 µL $TbCl_3$ were added to a glass round-bottom flask and stirred for 10 min. Next, 3 mL $Na_5P_3O_{10}$ was added rapidly at room temperature producing a translucent solution after 5 min of stirring. The flask was transferred to an 80 °C oil bath and stirred for 3 hours. The nanoparticles were pelleted in a 15-mL disposable centrifuge tube and the supernatant was removed. The resulting pellet of nanoparticles was then subjected to the same poly(acrylic acid) wrapping and dialysis as described above for the YVO_4 nanoparticles.

Microfluidic mold fabrication

Fabrication of the master molds for the bead synthesizer was completed using standard photolithography techniques for multi-layer microfluidics on 4” silicon test-grade wafers similar to previous reports[2], including the fabrication of a multi-layer flow mold and a control mold.

For both molds, designs are available upon request. The control mold was fabricated using SU-8 2025 (MicroChem) according to the manufacturer's instructions for creating ~25 μm thick channels. Flow molds were constructed with multiple layers of positive (AZ 50XT, Capitol Scientific, Austin, TX) and negative (SU-8 2005, 2025, and 2050, MicroChem) photoresists for rounded valve regions and rectangular flow regions, respectively; a schematic showing the flow mold fabrication is provided in **Fig. S15**. Layer 0 consists of a uniform SU-8 2005 layer created using whole wafer flood exposure according to manufacturer's instructions for help with adhesion and multi-layer stability. Layer 1 consists of the rectangular water input resistors of ~5 um in height. Layer 2 consists of ~50 μm rounded valve regions in positive (AZ 50XT) photoresist. Layer 1 and 2 are developed before proceeding to Layer 3-5. Layer 3 consists of a 50 μm SU-8 2050 layer for the lanthanide inputs, the underlying mixer channel, and oil channels. Layer 4 consists of a 25 μm thick SU-8 2025 layer on top of layer 3 defining tall features throughout the mixer and T junction region of the device, with a total feature height of ~75 μm for this layer. Layer 5 consists of a 35 μm thick SU-8 2025 layer, defining ridges in the herringbone mixers for a total herringbone height of ~110 μm. Layers 3-5 are co-developed in an ending step before a final hard bake.

Microfluidic mold fabrication detailed protocol

Layer 1: Flow resistors (SU-8 2005). Spin-coat: (1) 500 rpm for 10 s, 133 rpm s^{-1} accl. (2) 2800 rpm for 40 s, 266 rpm s^{-1} accl. (cast). Soft bake: 65°C 2 min/95°C 3 min/65°C 2 min. UV exposure: 20 s at 8.2 mW cm^{-2} . Post exposure bake: 65°C 2 min/95°C 4 min/65°C 2 min. Develop: 30 s in SU-8 Developer (Microchem).

Layer 2: Rounded valves (AZ 50XT). Spin-coat: (1) 200 rpm for 6 s, 133 rpm s^{-1} accl. (2) 1400 rpm for 35 s, 266 rpm s^{-1} accl, (3) 3400 rpm for 1 s with 1 s ramp at top speed (edge bead removal). Relax: 20 min. Soft bake: 65°C - 112°C full speed ramp for 22 min. Rehydrate 3 hours in a wet box. UV exposure: 25 s x 5 with 30 s pauses in between at 8.2 mW cm^{-2}. Develop: 1:3 solution of AZ Electronic Materials AZ 400K developer (Capitol Scientific). Hard bake: ramp from 65°C to 190°C at 10°C hr^{-1}, remain at 190°C for 4 hrs, for 15 hours total.

Layer 3: Low rectangular flow layer (SU-8 2050) Spincoat: (1) 500 rpm for 10 s, 133 rpm s^{-1} accl. (spread), (2) 3000 rpm for 36 s, 399 rpm s^{-1} (cast). Relax: 20 min. Soft bake: 65°C 2 min/95°C 10 min/65°C 2 min. UV exposure: 29 s at 8.2 mW cm^{-2}. Post exposure: 65°C 2 min/95°C 10 min/65°C 2 min. No development.

Layer 4: High rectangular flow layer (SU-8 2025) Spin-coat: (1) 500 rpm for 10 s, 133 rpm s^{-1} accl. (spread), (2) 3500 rpm for 36 s, 399 rpm s^{-1} accl. (cast). Relax: 10 min. Soft bake: 65°C 2 min/95°C 8 min/65°C 2 min. UV exposure: 32 s at 8.2 mW cm^{-2}. Post-exposure bake: 65°C 3 min/95°C 6 min/65°C 2 min. No development.

Layer 5: Herringbone ridge layer (SU-8 2025) Spin-coat: (1) 500 rpm for 10 s (spread), 133 rpm s^{-1} accl. (2) 2500 rpm for 35 s, 399 rpm s^{-1} accl. (cast). Relax: 10 min. Soft bake: 65°C 2 min/95°C 8 min/65°C 2 min. UV exposure: 24 s at 8.2 mW cm^{-2}. Post-exposure bake: 65°C 2 min/95°C 6 min/65°C 2 min.

Final Development: Layers 3-5 were co-developed for 6 min 30 s in SU-8 Developer, followed by hard baking for 2 hours at 165°C, with an initial ramp from 65°C to 165°C at 120°C hr^{-1}.

Microfluidic device fabrication

Microfluidic devices were fabricated as previously reported[2]. Soft polymer devices were cast using the master molds under standard PDMS procedures. Each bead synthesizer device was fabricated in a soft-polymer plastic (RTV 615, Momentive) with a flexible control layer (1:20 curing agent: elastomer base polymer ratio) on top of a flow layer (1:5 curing agent: elastomer base polymer ratio), allowing the fluidic channels to be controlled by active valving as described in the text.

Microfluidic device operation

Valves in the microfluidic devices were actuated by 10 mm pneumatic solenoid valves (Festo Corp., Hauppauge, NY) driven by an ethernet-based, programmable fieldbus I/O system with digital output modules (750-841 Programmable Fieldbus Controller, 750-504 4-Channel Digital Output Module, Wago Corp., Germantown, WI). All fluids were injected into the microfluidic devices using pressure-driven flow from custom-made containers. Pressurized air to operate the valves was passed from the house air supply through a series of high efficiency filters for oil and particulate removal. Air pressure for pressure-driven flow of fluids into the chips was supplied by a high precision pressure control system (MFCS-EZ, Fluigent, Inc., Lowell, MA). A custom software platform written in MATLAB (The MathWorks Inc., Natick, MA), with a graphical user interface, allowed for real time control and script-driven automation of all aspects of the chip operation.

Bead synthesis

Encoded beads were generated by adjusting input pressures to vary relative ratios of 5 different monomer lanthanide input solutions while keeping the overall flow rate constant. All monomer input solutions contained a mixture of double-distilled water (ddH_2O), 42.8% v/v 700 MW PEG-diacrylate (Sigma-Aldrich), 39.2 mg mL^{-1} lithium phenyl-2,4,6-trimethylbenzoylphosphinate (LAP) [43], and 5.0% v/v YVO_4:Eu (at 25 mg mL^{-1}). Input Sm and Dy solutions also contained 16.3% v/v of YVO_4:Sm (25 mg mL^{-1}) and YVO_4:Dy (25 mg mL^{-1}), respectively; Tm and CeTb input solutions contained 16.3% v/v of YVO_4:Tm (12.5 mg mL^{-1}) and $LaPO_4$:CeTb (12.5 mg mL^{-1}), respectively. All lanthanide solutions used in the monomer input solutions were obtained by diluting 50 mg/mL stock solutions (in water) to the concentrations listed above by dilution with 0.1 M HEPES, pH 6.8. The LAP concentration used is the minimum required to achieve reliable on-chip bead polymerization; higher LAP concentrations reduced lanthanide brightness. We had previously observed photodamage of the bead synthesis device due to long exposures (days) to UV light, as evidenced by darkening of the PDMS where it was exposed to UV. Replacement of the previous photoinitiator, Irgacure 2959, with LAP eliminated this photodamage, presumably because the more hydrophilic LAP does not diffuse into the PDMS.

Lanthanide input solutions were mixed via passage through a herringbone channel and flowed through a T-junction into a continuous stream of light mineral oil (Sigma-Aldrich) containing 2% v/v Abil EM 90 (Evonik Industries, Germany) and 0.05% v/v Span 80 (Sigma-Aldrich) as surfactants to form droplets[2]. Droplets were then photopolymerized into beads with a spot of UV light focused onto the output channel below the T-junction. The UV spot was generated by imaging the tip of a 3mm diameter UV liquid light guide onto the microfluidic device at 1:1 magnification. The UV light source was either a full-spectrum 300W Xenon arc lamp (Newport,

Irvine, CA), reflected off a 400 nm long pass mirror (CVI Melles-Griot, Albequerque, NM) or a Lambda LS Xenon arc lamp (Sutter, Novato, CA) with a custom cold mirror to reflect UV light into the liquid light guide. Precision pressure controllers (MFCS-EZ, Fluigent, Inc., Lowell, MA) were used to control the lanthanide flow rates by controlling the air pressure over stock lanthanide solutions. Calibration of pressure to flow rate for each input was performed as described previously.

Bead Imaging

Beads were imaged on a custom Nikon Ti microscope with a UV transilluminator as described previously[2], except that the liquid light guide used to connect the lamp to the microscope was imaged onto the bead sample to form a 3mm diameter spot. The same illuminator was used for both UV excitation of the beads and brightfield imaging. Beads suspended in phosphate buffered saline containing 0.1% Tween 20 (pH = 7.4) were spread on a quartz slide and covered with a quartz coverslip prior to imaging. The filter sets used for lanthanide imaging and unmixing were (all purchased from Semrock, Rochester, NY): 435/40, 474/23 and 473/10, 527/20, 536/40, 546/6, 572/15, 620/14, 630/92, 650/13. The 473/23 and 473/10 filters were combined because the 473/10 filter does not block light beyond 650 nm, while the 474/23 filter blocks light to beyond 950 nm. The narrower 473/10 filter improves separation of the YVO_4:Dy emission from the YVO_4:Tm emission.

Image analysis

Linear unmixing of the acquired images to determine lanthanide intensity images was performed using standard least squares fitting to express the measured image stack as the sum of each lanthanide image multiplied by its reference spectrum. In contrast to our previous work, background subtraction and flat-fielding of the images were not performed, as these corrections did not improve bead classification accuracy. Reference spectra for each lanthanide were measured from beads containing single lanthanide species, and a background spectrum was determined from a bead-free region of an image from each imaging session. Beads were identified from brightfield images using the circular Hough transform. Pixels corresponding to each bead in the remaining images were then defined using the centroid position returned by the Hough transform and a circular radius chosen to be smaller than the smallest identified bead. Each bead subtends ~ 75 pixels in our images; therefore, choosing a mask with a radius slightly smaller than the smallest bead does not affect the noise characteristics of the measurement. For each bead, the median intensity of each lanthanide was recorded, as was the median ratio of each lanthanide intensity to the intensity of the Eu internal standard. For a given data set, corresponding to a set of images of MRBLEs from a single code imaged in a single session, the unmixed intensities for the entire set of beads was extracted. Beads whose fluorescence in the background channel deviated by more than three standard deviations from the mean were rejected to remove beads overlapping with autofluorescent dust. Beads whose fluorescence in the Eu channel deviated by more than three standard deviations from the mean (for MRBLEs with a single Eu level) or beads with less than a minimum Eu intensity (for MRBLEs with multiple Eu levels) were rejected to eliminate incorrectly identified beads. These filters typically eliminated <0.5% of beads. Lanthanide ratios for the beads passing these filters were registered to the programmed codes by fitting a transformation matrix and offset to the entire bead data set using an Iterative Closest Point matching algorithm as described previously.

The scaling matrix allows stretching of the lanthanide ratios along each axis as well as shearing and rotation. To classify beads, a Gaussian mixture model was fit to the transformed lanthanide ratio intensities. This determines both the most likely code identity for each bead and the parameters which best describe the distribution of ratio intensities in each code. All data analysis was carried out in Matlab (Mathworks, Natick MA). For this approach, we accounted for variations in lamp intensity by normalizing the measured absolute Eu intensity of each bead to the bead intensity within the brightfield image for the same bead. The remaining variation is relatively small (<10%) (**Figure S8**), suggesting that beads containing three widely separated levels of Eu should be separable on the basis of the Eu brightness.

Prediction of resolvable code levels

The target lanthanide ratios that define the codes in a MRBLE code set are determined by calculating those ratios that are expected to be separated from each other by a user-specified number of standard deviations, based on the measured dependence of code cluster standard deviations on code cluster mean from a previous MRBLE code set. After fitting a Gaussian mixture model to the lanthanide ratios measured from a MRBLE code set, the diagonal entries of the covariance matrix give the variance of each Gaussian cluster along the principal axes (the lanthanide ratios). The square root of these diagonal entries is the standard deviation of each code along these axes. We then fit a linear model of the standard deviation for each lanthanide as a function of the lanthanide means. This linear model allows us to predict the standard deviation of a code cluster based on its position. We use these linear models to choose code coordinates on each axis that place each code cluster a constant number of standard deviations from its neighbors. Specifically, for two codes with means μ_1, μ_2 and standard deviations σ_1, σ_2, we want $\mu_1 + n\sigma_1 = \mu_2 - n\sigma_2$, where n is the number of standard deviations to separate the codes by. If $\sigma = \sigma_0 + c\mu$, where σ_0 is the standard deviation at zero lanthanide concentration and c is the slope of the line, we can solve for μ_2 given μ_1 as

$$\mu_2 = \frac{(1 + nc)\mu_1 + 2\eta\sigma_0}{1 - nc}$$

Using this expression, we calculate levels for each lanthanide ratio recursively starting at zero lanthanide concentration and continuing until the next lanthanide ratio would be greater than 1. By adjusting n, we can control the separation between clusters and the number of codes we can generate.

Section 2: Supplemental Tables

	Lanthanide Mean	*Estimate*	*p Value*
CeTb SD	Intercept	0.0066 ± 0.0011	3.5e-08
	CeTb	0.0628 ± 0.0019	2.3e-56
	Dy	0.0002 ± 0.0031	0.95
	Sm	0.0001 ± 0.0028	0.98
	Tm	-0.0016 ± 0.0023	0.50
Dy SD	Intercept	0.0020 ± 0.0002	6.9e-13
	CeTb	-0.0004 ± 0.0004	0.38
	Dy	0.0195 ± 0.0007	8.3e-50
	Sm	0.0000 ± 0.0006	0.98
	Tm	-0.0001 ± 0.0005	0.87
Sm SD	Intercept	0.0031 ± 0.0003	5.5e-22
	CeTb	-0.0005 ± 0.0004	0.28
	Dy	-0.0003 ± 0.0007	0.69
	Sm	0.0184 ± 0.0006	4.1e-51
	Tm	-0.0010 ± 0.0005	0.055
Tm SD	Intercept	0.0031 ± 0.0004	3.5e-13
	CeTb	0.0000 ± 0.0006	0.97
	Dy	0.0230 ± 0.0010	1.1e-40
	Sm	-0.0011 ± 0.0009	0.22
	Tm	0.0319 ± 0.0008	1.2e-64

Table S1: Results of regression of lanthanide standard deviation vs. mean. Linear regressions were calculated with the fitlm command in Matlab from the data shown in **Fig. 3.** Statistically significant relationships are highlighted in bold.

# of codes	***# of levels of*** *Eu / CeTb / Dy / Sm / Tm*	***# of beads*** *analyzed*	***% of beads identified at confidence level*** *99.99%*	*99.9%*
106	1 / 2 / 6 / 6 / 5	3213	100%	100%
285	1 / 3 / 8 / 7 / 6	11655	100%	100%
341	1 / 5 / 8 / 7 / 5	46387	99.97%	99.98%
551	1 / 4 / 9 / 7 / 7	24407	99.1%	99.5%
1023	3 / 5 / 8 / 7 / 5	40439	99.8%	99.94%
1101	2 / 4 / 9 / 7 / 7	50654	98.0%	99.1%

Table S2: Summary of MRBLE sets synthesized and imaged in this work.

Section 3: Additional Data and Resources

AutoCad files are available upon request from the authors.

Section 4: Supplementary References

[1] B. D. Fairbanks, M. P. Schwartz, C. N. Bowman, K. S. Anseth, *Biomaterials* **2009**, *30*, 6702.
[2] R. E. Gerver, R. Gómez-Sjöberg, B. C. Baxter, K. S. Thorn, P. M. Fordyce, C. A. Diaz-Botia, B. A. Helms, J. L. DeRisi, *Lab Chip* **2012**, *12*, 4716.
[3] V. Buissette, D. Giaume, T. Gacoin, J.-P. Boilot, *J. Mater. Chem.* **2006**, *16*, 529.
[4] V. Buissette, M. Moreau, T. Gacoin, J.-P. Boilot, J.-Y. Chane-Ching, T. Le Mercier, *Chem. Mater.* **2004**, *16*, 3767.

Section 5: Supplementary Figures

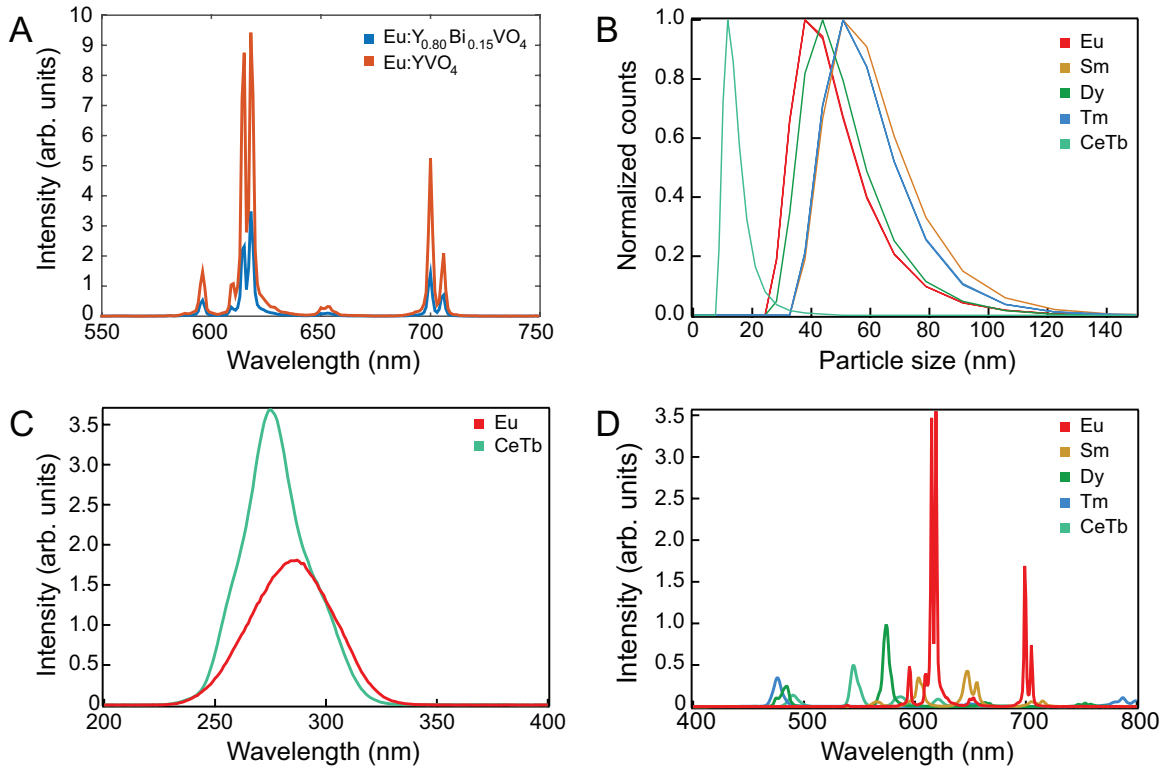

Figure S1. Properties of lanthanide nanophosphors (LNs) used for spectral encoding. **(A)** Emission spectra (absolute scale) demonstrating increased emission intensity following removal of Bi co-dopant from Eu:YVO_4 nanophosphors. **(B)** Representative size distributions of synthesized Schematic showing steps for fabricating microfluidic flow molds on silicon wafers. **(C)** Excitation spectra of Eu:YVO_4 and CeTb:$LaPO_4$ plotted on an absolute scale. **(D)** Emission spectra of all lanthanide nanophosphors used in this paper plotted on an absolute scale to demonstrate relative brightness.

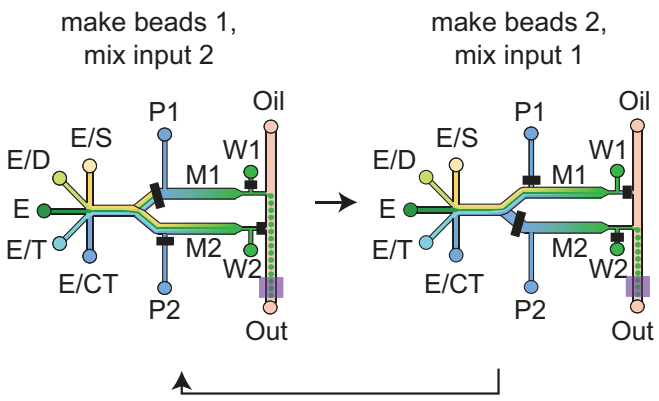

Figure S2. Cartoon showing two-step microfluidic MRBLE production process. E/S, E/D, E, E/T, and E/CT are the LN/polymer inputs; M1 and M2 are mixers 1 and 2; P1 and P2 are push water for mixers 1 and 2; and W1 and W2 are the waste outputs from mixers 1 and 2. Black bars indicate closed valves. After filling mixer 1, mixer 2 is filled while MRBLEs are produced from mixer 1 (left). MRBLEs are then produced from mixer 2 while mixer 1 is washed and refilled (right). The cycle repeats until all MRBLE codes are produced.

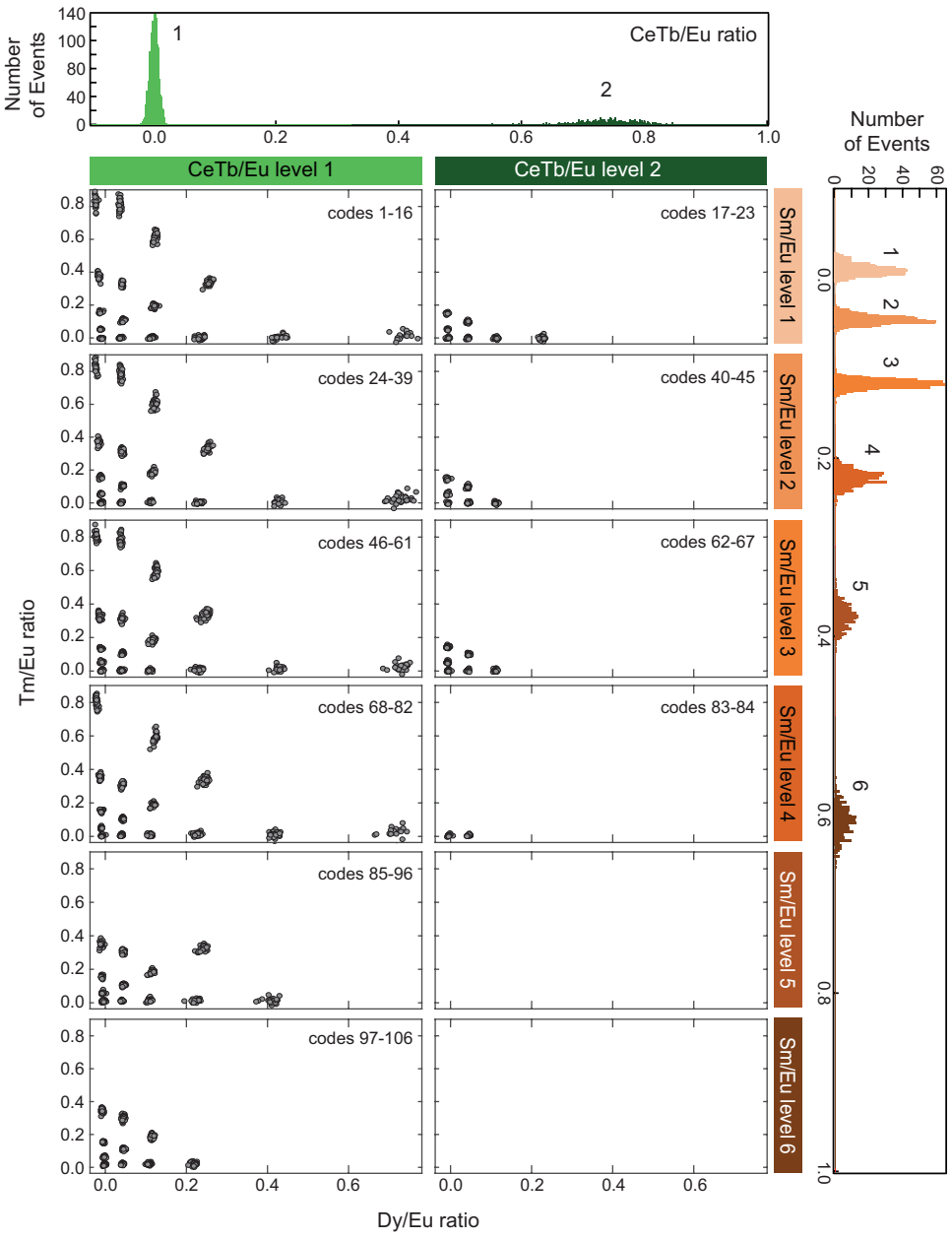

Figure S3: Scatter plot of the measured intensity ratios for 3,185 MRBLEs from a 106-code set. MRBLEs are first separated by CeTb/Eu ratio (2 columns, with each column corresponding to a single peak within the histogram of all CeTb/Eu intensities shown at top) and Sm/Eu ratio (7 rows, with each row corresponding to a single peak within the histogram of all Sm/Eu intensities shown at right). For each unique combination of CeTb/Eu and Sm/Eu ratios, a panel displays Tm/Eu ratios plotted vs Dy/Eu ratios to show individual clusters.

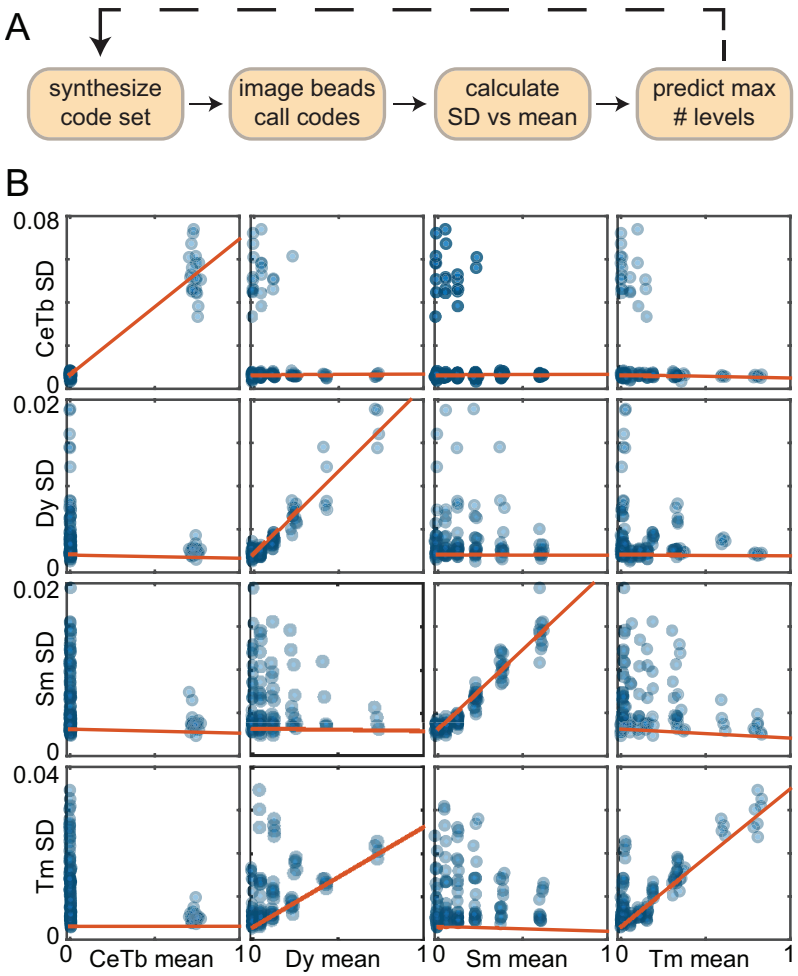

Figure S4: Experimental determination of variables affecting code cluster standard deviation (SD). **(A)** General scheme for recursive prediction of minimum distinguishable intensity level spacing within large code sets. **(B)** Plots of LN ratio SD vs mean for each code cluster within the 106-code MRBLE set. SDs and means were determined from the Gaussian mixture model fit to the data shown in **Figure S3**. Each point in these plots corresponds to one cluster in the code set; subplot rows show individual LN SD values; subplot columns show individual LN mean values; and orange lines show linear regression models for each SD/mean pair. The SD of each LN ratio cluster is well predicted by the mean ratio of that LN with the exception of Tm/Eu; for Tm/Eu, the SD of each code cluster depends on both mean Tm/Eu level and mean Dy/Eu level.

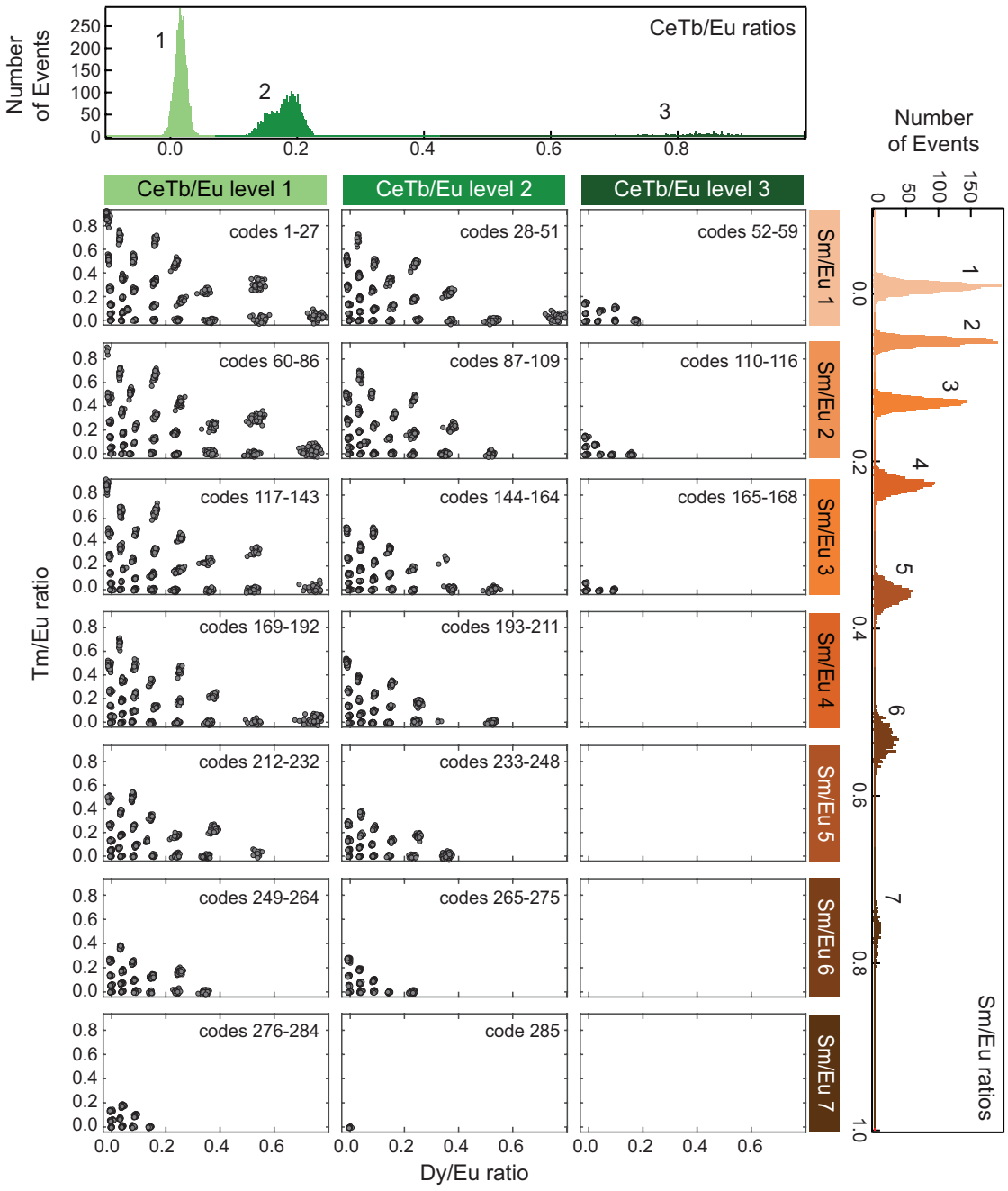

Figure S5: Scatter plot of the measured ratios of 11,655 MRBLEs from a 285 code set. MRBLEs are first separated by CeTb/Eu ratio (3 columns, with each column corresponding to a single peak within the histogram of all CeTb/Eu intensities shown at top) and Sm/Eu ratio (7 rows, with each row corresponding to a single peak within the histogram of all Sm/Eu intensities shown at right). For each unique combination of CeTb/Eu and Sm/Eu ratios, a panel displays Tm/Eu ratios plotted vs Dy/Eu ratios to show individual clusters.

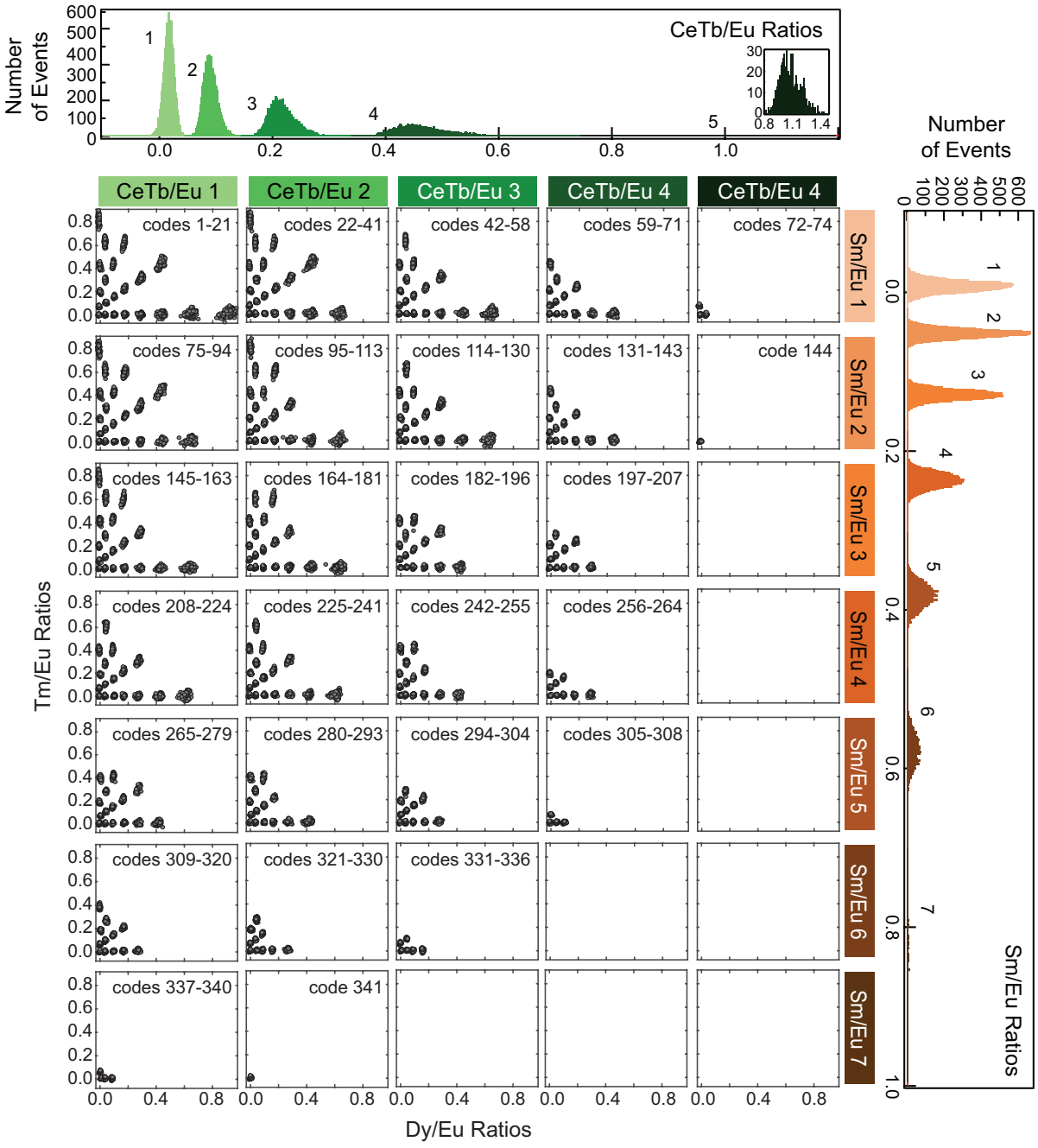

Figure S6: Scatter plot of the measured ratios from a 341 code MRBLE set. 10% of the 46387 MRBLEs are plotted to reduce crowding and improve visualization. MRBLEs are first separated by CeTb/Eu ratio (5 columns) and Sm/Eu ratio (7 rows); for each unique combination of CeTb/Eu and Sm/Eu ratios, a panel displays Tm/Eu ratios plotted vs Dy/Eu ratios to show individual clusters. There are few beads in the CeTb/Eu level 5 cluster; therefore, we include a zoomed histogram of this level for clarity.

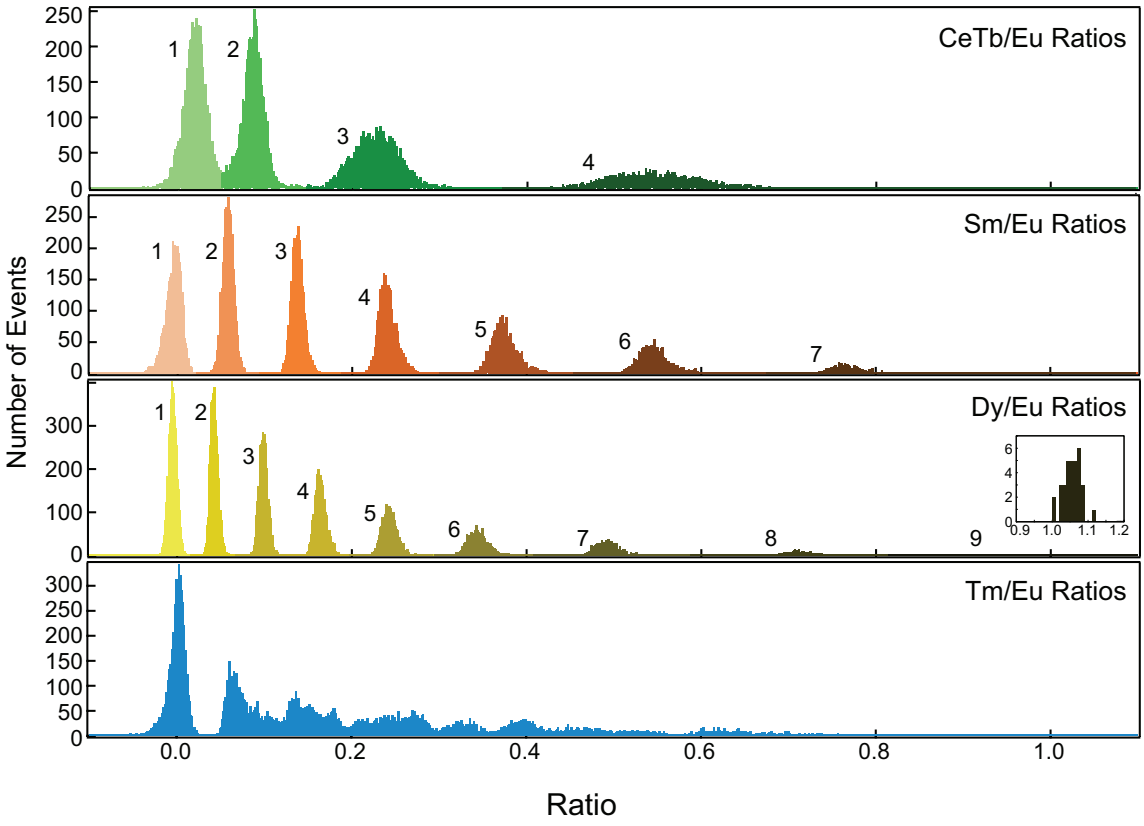

Figure S7: Histograms of measured CeTb/Eu, Dy/Eu, Sm/Eu, and Tm/Eu ratios from a 550 code MRBLE set. CeTb/Eu, Dy/Eu, and Sm/Eu histograms show clear peaks; measured Tm/Eu intensities do not show clearly defined peaks because target Tm/Eu levels do not lie on an orthogonal grid. Dy/Eu level 9 contains a small number of beads; therefore, this cluster is shown as an inset.

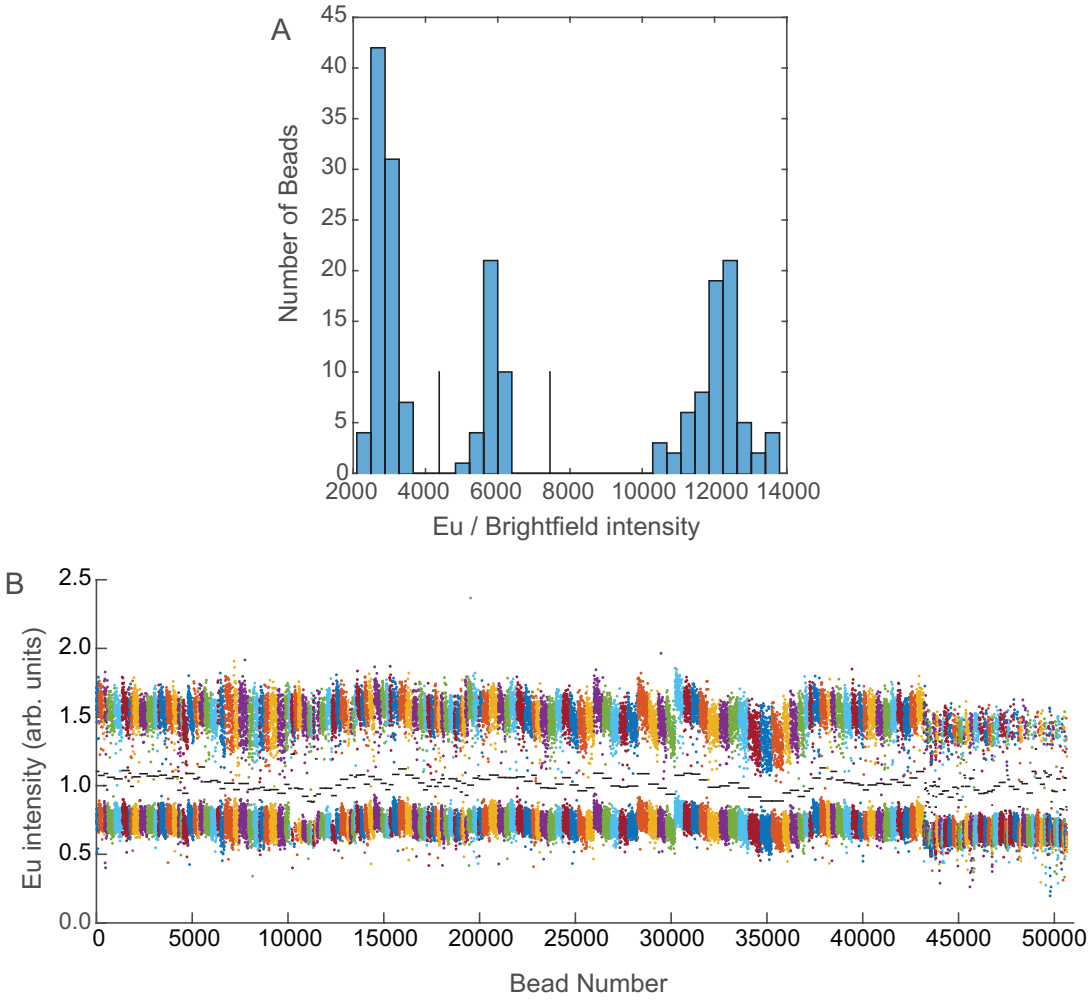

Figure S8: Distinguishing variable Eu levels used as an additional coding variable. **(A)** Histogram of absolute Eu intensities, normalized by the bright field intensity, for one image of the 1,023 code set. Vertical black lines indicate the boundaries between codes as fit by a Gaussian mixture model; a MRBLE with an intensity on the line will be assigned to the two clusters on either side of the line with equal probability. **(B)** Separation of all Eu intensities in the 1101-code MRBLE over all images. Each point corresponds to a single MRBLE, and each image is plotted in a different color. The black lines represent the fitted boundary between the two Eu levels for each image.

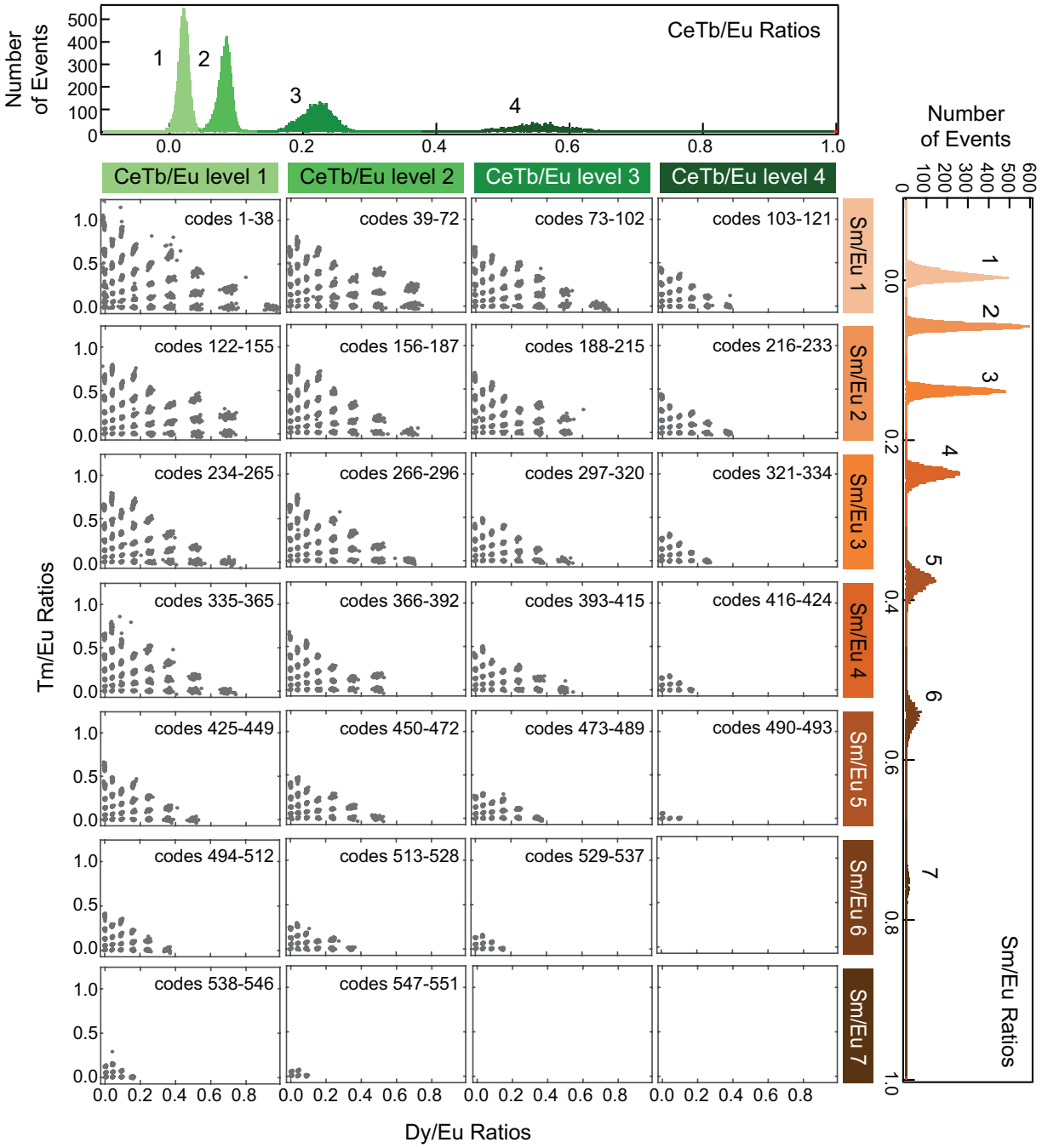

Figure S9: Scatter plot of the 551 codes comprising the low Eu level of the 1102-code MRBLE set.

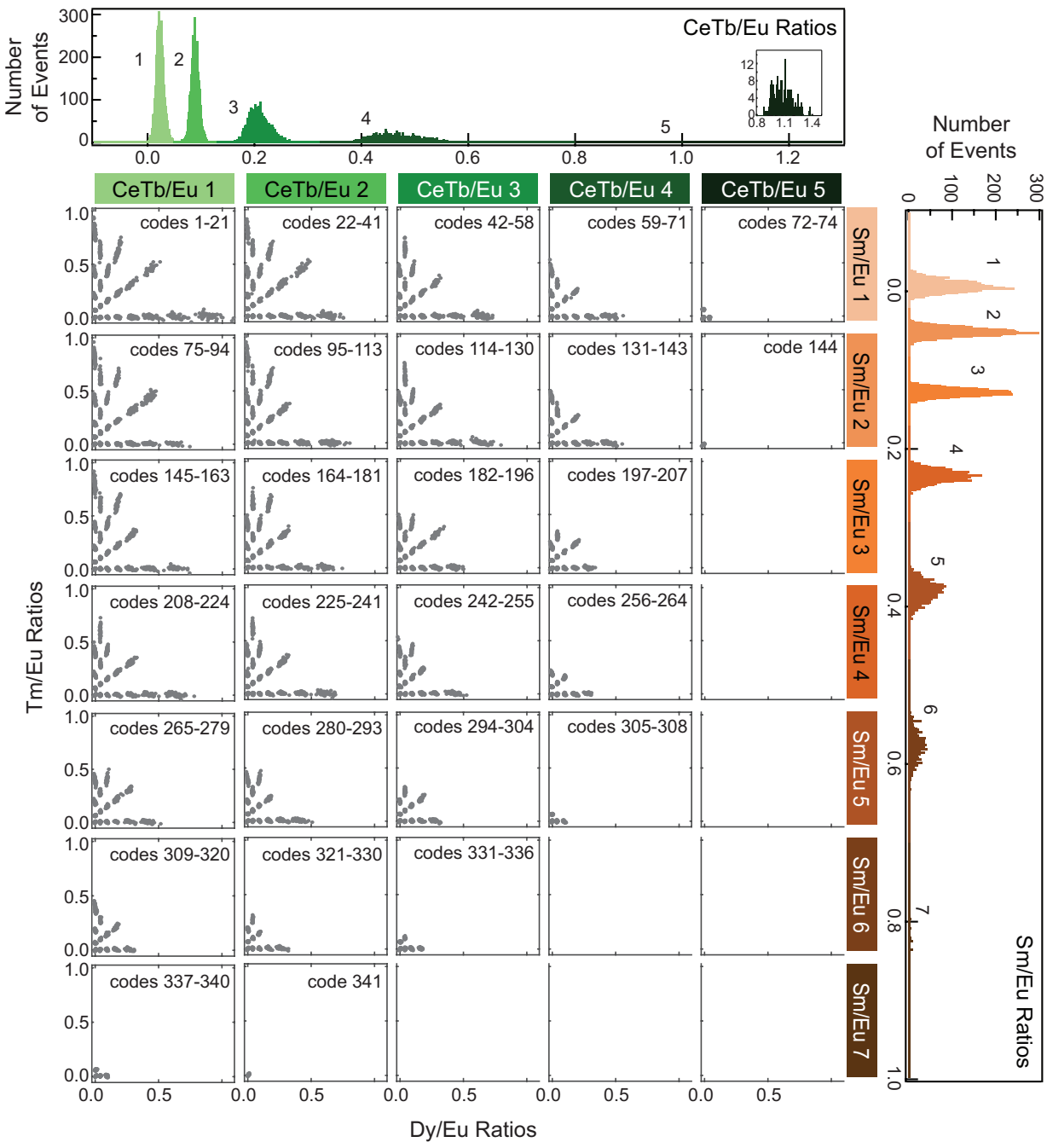

Figure S10: Scatter plot of 341 Code set from 25% Eu level from 1023-code MRBLE set. MRBLEs are first separated by CeTb/Eu ratio (5 columns) and Sm/Eu ratio (7 rows); for each unique combination of CeTb/Eu and Sm/Eu ratios, a panel displays Tm/Eu ratios plotted vs Dy/Eu ratios to show individual clusters. There are few beads in the CeTb/Eu level 5 cluster; therefore, we include a zoomed histogram of this level for clarity.

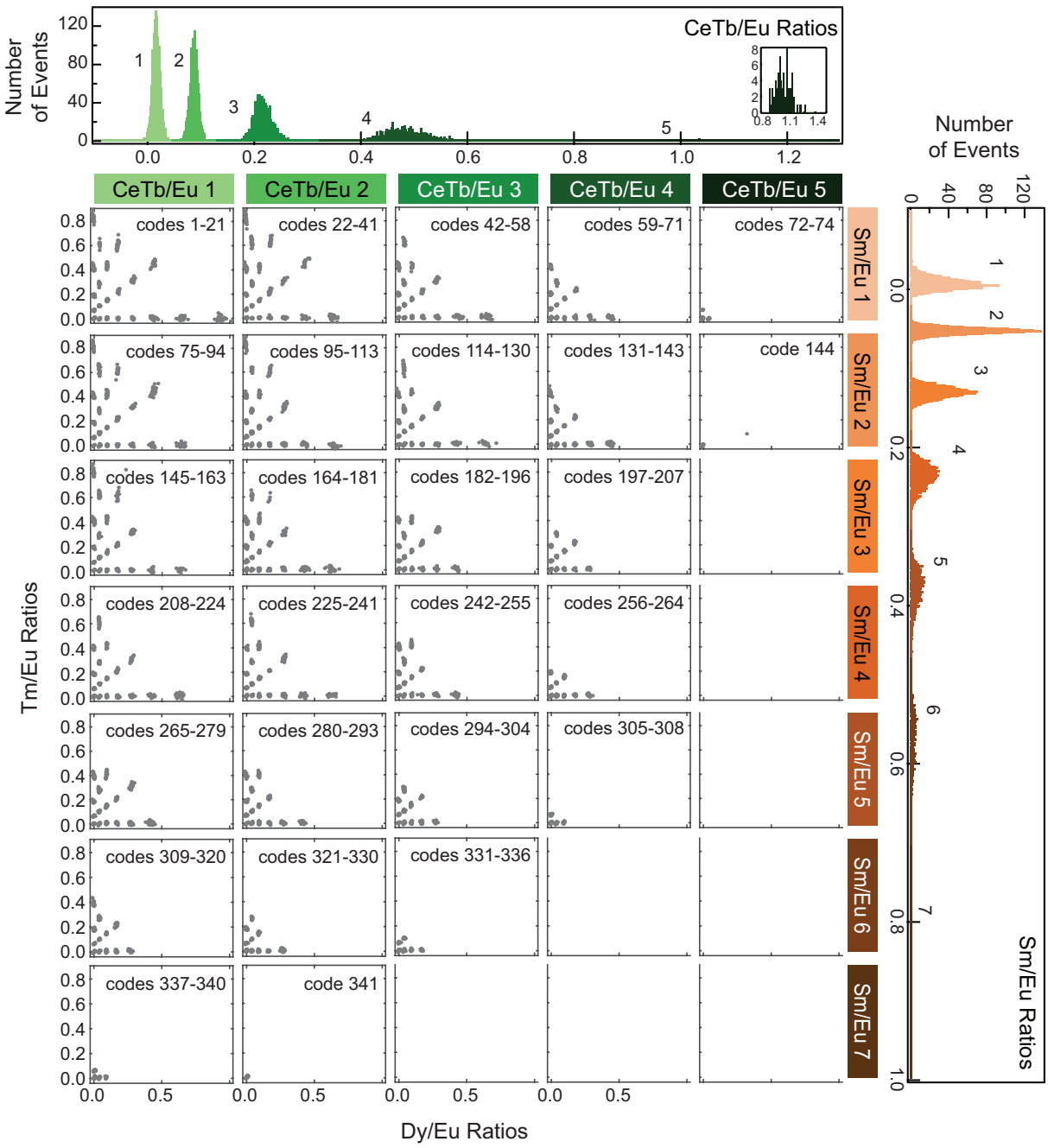

Figure S11: Scatter plot of 341 Code set from 50% Eu level from 1023-code MRBLE set. MRBLEs are first separated by CeTb/Eu ratio (5 columns) and Sm/Eu ratio (7 rows); for each unique combination of CeTb/Eu and Sm/Eu ratios, a panel displays Tm/Eu ratios plotted vs Dy/Eu ratios to show individual clusters. There are few beads in the CeTb/Eu level 5 cluster; therefore, we include a zoomed histogram of this level for clarity.

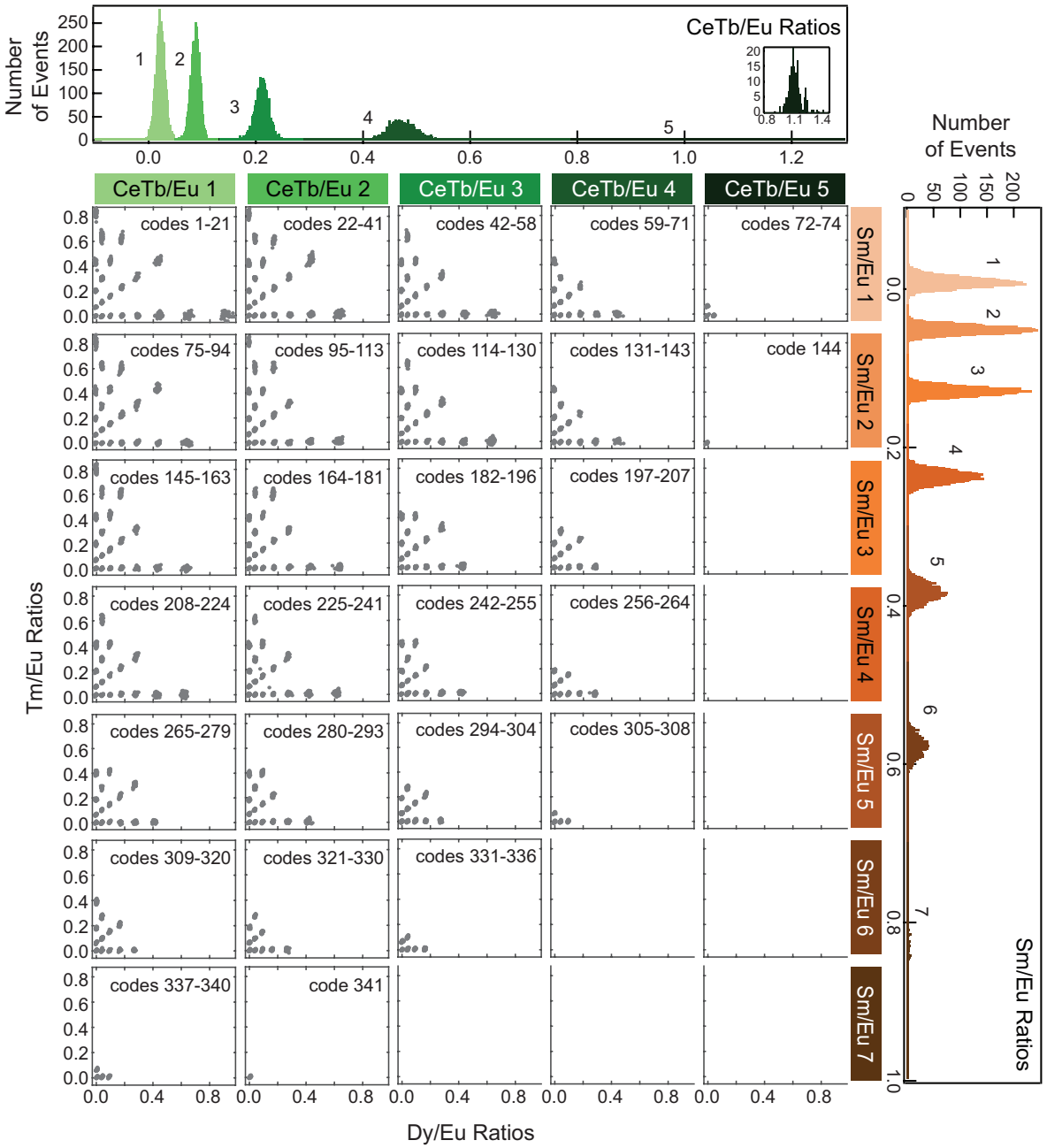

Figure S12: Scatter plot of 341 Code set from 100% Eu level from 1023-code MRBLE set. MRBLEs are first separated by CeTb/Eu ratio (5 columns) and Sm/Eu ratio (7 rows); for each unique combination of CeTb/Eu and Sm/Eu ratios, a panel displays Tm/Eu ratios plotted vs Dy/Eu ratios to show individual clusters. There are few beads in the CeTb/Eu level 5 cluster; therefore, we include a zoomed histogram of this level for clarity.

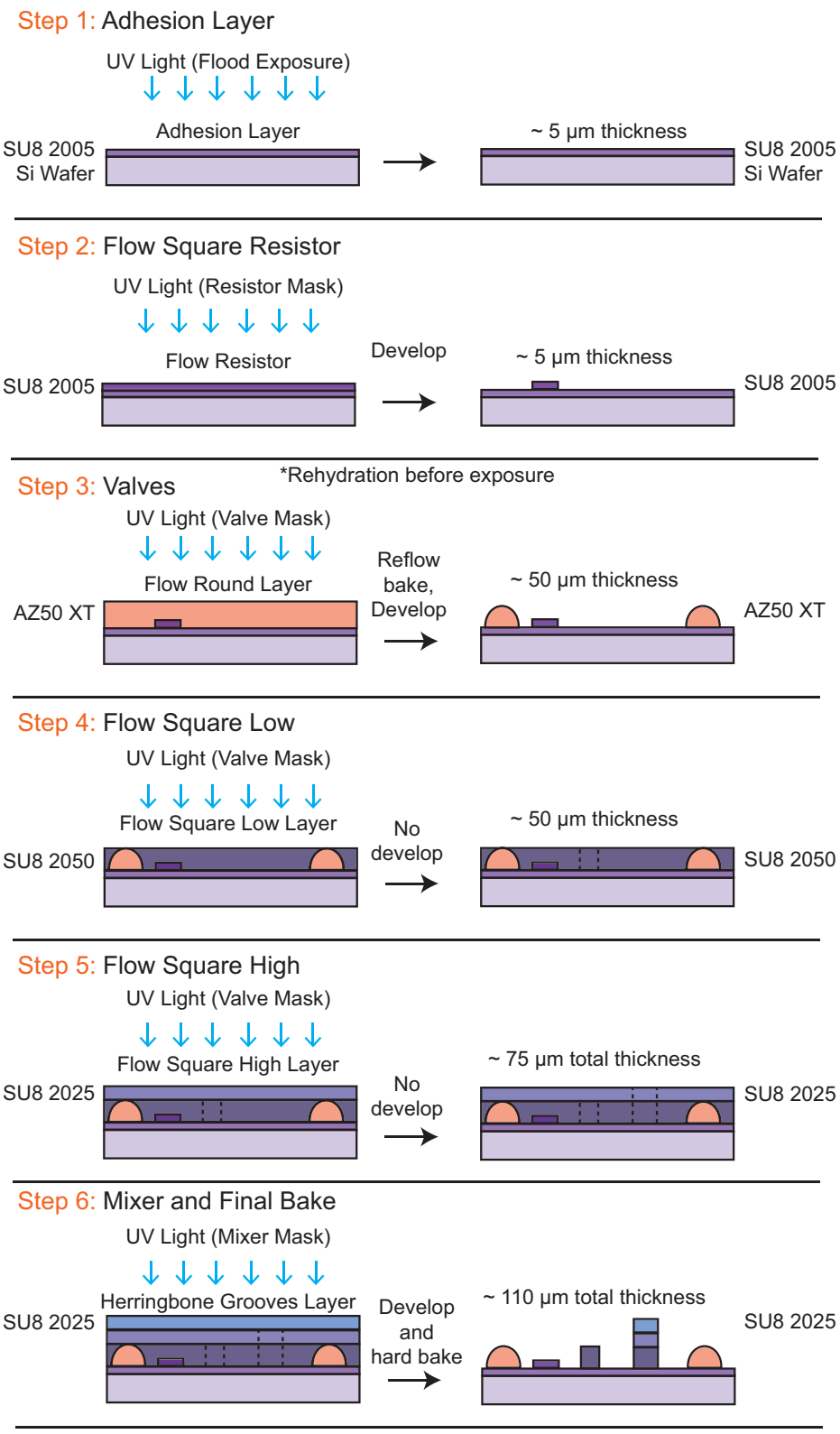

Figure S13: Schematic showing steps for fabricating microfluidic flow molds on silicon wafers.